Optimal Voltage Phasor Regulation for Switching Actions in Distribution Systems

Michael Sankur, Roel Dobbe, Alexandra Von Meier, Emma M. Stewart, and Daniel B. Arnold

Abstract—The proliferation of Distributed Energy Resources (DER) presents both challenges and opportunities for utility operators to manage distribution systems more effectively. Though it is desirable to use Optimal Power Flow (OPF) formulations to manage DER, such abstractions have historically required the use of semidefinite relaxations when modeling unbalanced distribution systems. As it can be difficult to obtain tight relaxations when solving semidefinite OPFs, in this work we introduce an extension to a linear model of unbalanced power flow that is subsequently incorporated into an OPF formulation. We then apply this OPF to control the real and reactive power output of DER to minimize voltage phasor differences across switches, while maintaining proper voltage magnitudes throughout the feeder. In so doing, we ensure that large amounts of power will not be instantaneously transferred as a result of switching actions. Simulation results confirm the ability of the OPF to simultaneously minimize voltage phasor differences and regulate system voltage magnitudes.

I. INTRODUCTION

Coordination of a diverse set of Distributed Energy Resources (DER) presents many challenges to utility operators, who strive to ensure power of sufficient quality and quantity is available to retail customers at least cost. Such assets can vary in size and nature from rooftop PV units and larger PV arrays, to battery storage systems, and demand response resources. Lack of intelligent management and coordination of DER (distributed PV, specifically) has already resulted in financial impacts for customers and the utility in Hawaii [1]. However, DER could, under the correct operational control scenarios, provide numerous benefits to the grid, including voltage support, ancillary services [2] and, perhaps, new sets of services that were previously infeasible due to lack of controlability or observability.

In distribution systems, it is important to distinguish control strategies based on balanced and unbalanced analysis. Indeed, a variety of strategies for the management of DER presently exist in which decisions are based on knowledge of balanced distribution system models. Turitsyn et al. [3] considered a suite of distributed control strategies for reactive power compensation using four quadrant inverters. The work of [4] studies distributed voltage regulation in the absence of communication, relying on locally obtained information. In [5], a two-stage control architecture for voltage regulation is considered where distributed controllers inject power based on local sensitivity measurements. The authors of [6] study local voltage reference tracking with integral-type controllers, based

on local voltage measurements. The authors of [7] address voltage regulation and loss minimization through solving an Optimal Power Flow (OPF) problem, and address convexity issues using second order cone relaxations. The work of [8] also considers an OPF approach for voltage regulation in distribution networks by framing the decision-making process as a semidefinite program. The authors provide conditions under which the semidefinite relaxation of the non-convex power flow problem is tight in balanced circuits. It is worth noting that many of the aforementioned approaches can be traced back to the seminal work of [9], that introduced non-linear and linear-approximated recursive branch power flow models. Finally, several of the authors of this paper have considered solving balanced optimal power flow problems where decisions are made in the absence of a network model [10].

However, as since neither loads nor impedances on all three phases are necessarily close to equal, and individual controllable DER may only be connected to single phases, strategies that consider individual phases as well as their mutual coupling effects need to be considered. Approaches to coordinate DER in unbalanced distribution systems, while being critical to the practical application in real distribution systems and microgrids [2], are much less prevalent in the literature. While there is consensus about the physics-based models [11], using these in an optimization setting is challenging as the nonlinear nature of power flow equations introduces considerable complexity that can be prohibitive for optimal power flow (OPF) calculations. Perhaps the best known efforts have been put forth by Dall'Anese et. al [12], [13], who consider Semi-Definite Program (SDP) relaxations for OPF problems in unbalanced systems, but do not provide conditions under which feasibility and optimality are guaranteed. In addition to inefficient scaling as the problem size grows, the work of [14] points out that it becomes more difficult to find a tight relaxation as the ratio of constraints to network buses increases. A likely reason that more strategies focusing on coordination of distributed energy resources in unbalanced systems do not exist is the lack of suitable linear models that approximate three phase power flow.

A key feature of linear models that makes them so attractive to incorporate into DER control strategies lies in their versatility to enable new types of problems to be formulated and solved. In our previous works [15] [16], we proposed a linearized unbalanced power flow model that can be viewed as an extension of the *LinDistFlow* [9] linear approximation for balanced systems. This model was incorporated into an

OPF designed to balance voltage magnitudes in three phase systems. Such an activity, to our knowledge, cannot be formulated as an SDP.

Another emerging application to which unbalanced linearized power flow models may be applied (to manage DER) is to enable fast and safe switching of circuit elements in distribution systems. The ability to island/reconnect microgrids and reconfigure distribution feeders are seen as two important applications of future grids [17], [18]. Prior to opening or closing a switch, it is desireable to minimize the voltage phasor difference across the switch to ensure the distribution system is not overly disturbed by large instantenous power flows. The ability to "cleanly" switch elements into and out of a given system could allow for faster restoration of electrical services to critical loads following a disaster, or allow for damaged components to be isolated for repair or replacement.

While most typical distribution systems do not have the sensing equipment to monitor voltage *phasors*, the growing presence of distribution Phasor Measurement Units (PMUs), indicates that sufficient infrastructure may be in place in future grids to support control activities seeking to regulate feeder voltage phasors. In fact, a small, but growing, number of control applications that utilize phase angle measurements have started to appear in literature. The work of [19] proposed the use of voltage angle measurements to curtail overgeneration of renewables. Additionally, the authors of [20] considered voltage angle thresholds as criteria to connect renewable generation. Both works refer to this control activity as "Angle Constrained Active Management", or ACAM.

In order to enable a control strategy that can regulate voltage phasors, in this work we extend the previously studied model [15], [16] which we refer to as the *LinDist3Flow* system, to consider voltage phase angles, thereby allowing OPF formulations to manage voltage phasors rather as opposed to only magnitudes.

The specific activity studied herein is an OPF formulation that minimizes the voltage phasor difference across an open switch in a distribution system while simultaneously regulating feeder voltage magnitudes to within acceptable limits. In the event that one of the phasors is uncontrolled (i.e. a reference signal), then this activity can be though of as a voltage phasor tracking problem. In driving the voltage phasor difference across a circuit element to 0, we ensure that when the switch is closed, only small amounts of power will flow across this element. In this manner, the switch can be closed without disturbing the rest of the voltage profile in the feeder.

We first discuss the *Dist3Flow* equations and extend the system to model voltage angles in Section II. Here, we also apply simplifying assumptions to the extended *Dist3Flow* system to derive a linear model suitable for incorporation into an optimal power flow formulation (we refer to the linearized system as the *LinDist3Flow* model). Simulation results of an OPF that uses the *LinDist3Flow* system to track a voltage phasor reference at a specific point in the network, and regulate system voltage magnitudes are presented in Section III.

TABLE I: NOMENCLATURE

V_n^ϕ	Voltage phasor at node n on phase ϕ
$\mathbb{V}_n$	Vector of voltage phasors at node n
y_n^ϕ	Square magnitude of voltage at node n on phase ϕ
$\mathbb{Y}_n$	Vector of square magnitudes of voltage at node n
θ_n^ϕ	Phase angle of voltage phasor at node n on phase ϕ
$Z_{mn}^{\phi\phi}$	Impedance of segment (m,n) on phase ϕ
$Z_{mn}^{\phi\psi}$	Impedance of segment (m,n) between phases (ϕ,ψ)
$\mathbb{Z}_{mn}$	Impedance matrix of line segment (m,n)
I_n^ϕ	Current phasor entering node n on phase ϕ
$\mathbb{I}_n$	Vector of current phasors entering node n
i_n^ϕ	Load current of phase ϕ at node n
$\mathbf{i}_n$	Vector of load currents at node n
S_n^ϕ	Phasor of complex power entering node n on phase ϕ
$\mathbb{S}_n$	Vector of complex power phasors entering node n
s_n^ϕ	Complex load on phase ϕ at node n
$\mathbf{s}_n$	Vector of complex loads at node n
w_n^ϕ	Inverter complex dispatch on phase ϕ at node n
$(\cdot)^*$	Complex conjugate (transpose) of scalar (vector or matrix)

II. ANALYSIS

A. Preliminaries

Let $\mathcal{T} = (\mathcal{N}, \mathcal{E})$ denote a rooted tree graph representing an unbalanced radial distribution feeder, where $\mathcal{N}$ is the set of nodes of the feeder and $\mathcal{E}$ is the set of line segments. Nodes are indexed by $n = 0, 1, \ldots, N-1$, where N is the order (number of nodes) of the distribution feeder, and node 0 denotes the feeder head (or substation). We treat node 0 as an infinite bus, decoupling interactions in the downstream distribution system from the rest of the grid. While the substation voltage may evolve over time, we assume this evolution takes place independently of DER control actions in $\mathcal{T}$. Each node and line segment can have up to three phases, labeled a, b, and c. For convenience, phases are referred to by the variables ϕ and ψ, where $\phi \in \{a, b, c\}$, $\psi \in \{a, b, c\}$. The current/voltage relationship between adjacent nodes m and n is captured by Kirchhoff's Voltage and Current Laws (KVL and KCL):

$$\begin{bmatrix} V_m^a \\ V_m^b \\ V_m^c \end{bmatrix} = \begin{bmatrix} V_n^a \\ V_n^b \\ V_n^c \end{bmatrix} + \begin{bmatrix} Z_{mn}^{aa} & Z_{mn}^{ab} & Z_{mn}^{ac} \\ Z_{mn}^{ba} & Z_{mn}^{bb} & Z_{mn}^{bc} \\ Z_{mn}^{ca} & Z_{mn}^{cb} & Z_{mn}^{cc} \end{bmatrix} \begin{bmatrix} I_n^a \\ I_n^b \\ I_n^c \end{bmatrix} \tag{1}$$

$$\begin{bmatrix} I_m^a \\ I_m^b \\ I_m^c \end{bmatrix} = \begin{bmatrix} i_m^a \\ i_m^b \\ i_m^c \end{bmatrix} + \sum_{n:(m,n)\in\mathcal{E}} \begin{bmatrix} I_n^a \\ I_n^b \\ I_n^c \end{bmatrix}, \tag{2}$$

where $Z_{mn}^{\phi\psi} = r_{mn}^{\phi\psi} + jx_{mn}^{\phi\psi}$ (with $j = \sqrt{-1}$) denotes the complex impedance of line (m,n) across phases ϕ and ψ. We assume a complex load is served at each node, where the load on a phase $s_n^\phi = V_n^\phi (i_n^\phi)^* \in \mathbb{C}$ is defined as:

$$s_n^\phi (V_n^\phi) = s_n^\phi \left(A_{PQ,n}^\phi + A_{Z,n}^\phi \left| V_n^\phi \right|^2 \right) + w_n^\phi \tag{3}$$

where $A_{PQ,n}^\phi + A_{Z,n}^\phi = 1$, and $w_n^\phi = u_n^\phi + jv_n^\phi$ denotes the complex components of DER dispatch.

B. Dist3Flow: Power and Losses

For completness, we now present the derivation of the Dist3Flow power flow equations (see [10], [16]) between adjacent buses in an unbalanced distribution system. We begin with writing KVL for a line segment (m, n) and KCL at a node m:

$$\mathbb{V}_m = \mathbb{V}_n + \mathbb{Z}_{mn}\mathbb{I}_n \tag{4}$$

$$\mathbb{I}_m = \mathbf{i}_m + \sum_{n:(m,n)\in\mathcal{E}} \mathbb{I}_n \tag{5}$$

Right multiplying $\mathbb{V}_m$ by the complex conjugate transpose (denoted by *) of Equation (5) and plugging in (4) on the RHS results in:

$$\mathbb{V}_m\mathbb{I}_m^* = \mathbb{V}_m\mathbf{i}_m^* + \sum_{n:(m,n)\in\mathcal{E}} \mathbb{V}_m\mathbb{I}_n^*$$

$$= \mathbb{V}_m\mathbf{i}_m^* + \sum_{n:(m,n)\in\mathcal{E}} \mathbb{V}_n\mathbb{I}_n^* + \mathbb{Z}_{mn}\mathbb{I}_n\mathbb{I}_n^* \tag{6}$$

$$= \mathbb{V}_m\mathbf{i}_m^* + \sum_{n:(m,n)\in\mathcal{E}} \mathbb{V}_n\mathbb{I}_n^* + \mathcal{L}_{mn}, \tag{7}$$

where $\mathcal{L}_{mn} = \mathbb{Z}_{mn}\mathbb{I}_n\mathbb{I}_n^* \in \mathbb{C}^{3\times3}$ denotes the power loss matrix.

While (7) is a 3×3 matrix equation, we are only interested in the diagonal entries, which are the complex powers in each phase of the circuit. We collect these entries into a 3×1 vector equation, that yields a relation of the complex power flowing into node m in terms of node m demand, powers flowing into downstream nodes, and losses in downstream line segments:

$$\mathbb{S}_m = \mathbf{s}_m + \sum_{n:(m,n)\in\mathcal{E}} \mathbb{S}_n + \mathbb{L}_{mn} \tag{8}$$

where $\mathbb{L}_{mn} \in \mathbb{C}^3$ and $\mathbb{L}_{mn}(i) = \mathcal{L}_{mn}(i,i)$ for $i = 1, 2, 3$. Eq. (8) is nonlinear and non-convex. As in our previous works [15], [16] we introduce the following assumption:

A1: $\mathbb{L}_{mn}$ is constant $\forall(m,n)\in\mathcal{E}$

Applying **A1** to (8) gives a linear equation for conservation of complex power, the *LinDist3Flow* power equation. As in [9], we can further simplify this equation by selecting $\mathbb{L}_{mn} = [0, 0, 0]^T \ \forall(m,n)\in\mathcal{E}$, giving (9).

$$\mathbb{S}_m \approx \mathbf{s}_m + \sum_{n:(m,n)\in\mathcal{E}} \mathbb{S}_n \tag{9}$$

C. Dist3Flow: Magnitude Equations

In this section, we present the derivation of the Dist3Flow voltage magnitude equations (see [10], [16]). We do this to motivate the extension of the model to consider voltage angles in the following section, and to highlight a common structure shared between the voltage magnitude/complex power flow and voltage angle/complex power flow relationships.

To start, we consider (4) on edge $(m, n) \in \mathcal{E}$ and right multiply both sides by their respective complex conjugate transpose, resulting in the 3×3 matrix equation:

$$\mathbb{V}_m\mathbb{V}_m^* = \mathbb{V}_n\mathbb{V}_n^* + \mathbb{Z}_{mn}\mathbb{I}_n\mathbb{V}_n^* + \mathbb{V}_n\mathbb{I}_n^*\mathbb{Z}_{mn}^* + \mathbb{Z}_{mn}\mathbb{I}_n\mathbb{I}_n^*\mathbb{Z}_{mn}^*$$

$$= \mathbb{V}_n\mathbb{V}_n^* + 2\,\mathbf{Re}\left\{\mathbb{V}_n\mathbb{I}_n^*\mathbb{Z}_{mn}^*\right\} + \mathcal{H}_{mn}, \tag{10}$$

where $\mathcal{H}_{mn} = \mathbb{Z}_{mn}\mathbb{I}_n\mathbb{I}_n^*\mathbb{Z}_{mn}^* \in \mathbb{C}^{3\times3}$ denotes a matrix of higher order terms. Noticing that for the scalar current $\left(I_n^\phi\right)^* = S_n^\phi\left(V_n^\phi\right)^{-1} \in \mathbb{C}$, we can write (10) as:

$$\mathbb{V}_m\mathbb{V}_m^* = \mathbb{V}_n\mathbb{V}_n^* + \mathcal{H}_{mn} + \dots$$
$$2\,\mathbf{Re}\left\{\mathbb{V}_n \left[S_n^a(V_n^a)^{-1} \quad S_n^b\left(V_n^b\right)^{-1} \quad S_n^c(V_n^c)^{-1}\right] \mathbb{Z}_{mn}^*\right\}. \tag{11}$$

Now, we define $\gamma_n^{\phi\psi} = V_n^\phi\left(V_n^\psi\right)^{-1} \in \mathbb{C}$ as the ratio of voltages between phases ϕ and ψ at node n, where $\phi, \psi \in \{a, b, c\}$, and clearly $\gamma_n^{\phi\psi} = 1$ if $\phi = \psi$. Applying this to (11) results in:

$$\mathbb{V}_m\mathbb{V}_m^* = \mathbb{V}_n\mathbb{V}_n^* + \mathcal{H}_{mn} + \dots$$
$$2\,\mathbf{Re}\left\{ \begin{bmatrix} S_n^a & \gamma_n^{ab}S_n^b & \gamma_n^{ac}S_n^c \\ \gamma_n^{ba}S_n^a & S_n^b & \gamma_n^{bc}S_n^c \\ \gamma_n^{ca}S_n^a & \gamma_n^{cb}S_n^b & S_n^c \end{bmatrix} \mathbb{Z}_{mn}^* \right\}. \tag{12}$$

We now gather the diagonal entries of (12) and place them into a 3×1 vector equation. Defining the variable $y_n^\phi = |V_n^\phi|^2$, and the vector $\mathbb{Y}_n = \left[y_n^a,\ y_n^b,\ y_n^c\right]^T$, (12) becomes:

$$\mathbb{Y}_m = \mathbb{Y}_n + \mathbb{H}_{mn} + \dots$$
$$2\,\mathbf{Re}\left\{ \begin{bmatrix} (Z_{mn}^{aa})^*S_n^a + \gamma_n^{ab}\left(Z_{mn}^{ab}\right)^*S_n^b + \gamma_n^{ac}(Z_{mn}^{ac})^*S_n^c \\ \gamma_n^{ba}\left(Z_{mn}^{ba}\right)^*S_n^a + \left(Z_{mn}^{bb}\right)^*S_n^b + \gamma_n^{bc}\left(Z_{mn}^{bc}\right)^*S_n^c \\ \gamma_n^{ca}(Z_{mn}^{ca})^*S_n^a + \gamma_n^{cb}\left(Z_{mn}^{cb}\right)^*S_n^b + (Z_{mn}^{cc})^*S_n^c \end{bmatrix} \right\}, \tag{13}$$

where $\mathbb{H}_{mn} \in \mathbb{C}^3$ and $\mathbb{H}_{mn}(i) = \mathcal{H}_{mn}(i,i)$ for $i = 1, 2, 3$. Equation (13) can be restated by grouping the γ and impedance terms into a 3×3 matrix multiplied by a 3×1 vector of complex powers, which results in:

$$\mathbb{Y}_m = \mathbb{Y}_n + \mathbb{H}_{mn} + \dots$$
$$2\,\mathbf{Re}\left\{ \begin{bmatrix} (Z_{mn}^{aa})^* & \gamma_{ab}\left(Z_{mn}^{ab}\right)^* & \gamma_n^{ab}\left(Z_{mn}^{ac}\right)^* \\ \gamma_n^{ba}\left(Z_{mn}^{ba}\right)^* & \left(Z_{mn}^{bb}\right)^* & \gamma_n^{ab}\left(Z_{mn}^{bc}\right)^* \\ \gamma_n^{ca}\left(Z_{mn}^{ca}\right)^* & \gamma_n^{cb}\left(Z_{mn}^{cb}\right)^* & \left(Z_{mn}^{cc}\right)^* \end{bmatrix} \begin{bmatrix} S_n^a \\ S_n^b \\ S_n^c \end{bmatrix} \right\}. \tag{14}$$

We can now rewrite (14) in terms of active and reactive components $\mathbb{P}_n, \mathbb{Q}_n \in \mathbb{C}^3$:

$$\mathbb{Y}_m = \mathbb{Y}_n + \mathbb{M}_{mn}\mathbb{P}_n + \mathbb{N}_{mn}\mathbb{Q}_n + \mathbb{H}_{mn}, \tag{15}$$

where the elements of $\mathbb{M}_{mn}$ and $\mathbb{N}_{mn}$ are defined as:

$$\mathbb{M}_{mn}(\phi, \psi) = 2\,\mathbf{Re}\left\{\gamma_n^{\phi\psi}\left(Z_{mn}^{\phi\psi}\right)^*\right\} \tag{16}$$

$$\mathbb{N}_{mn}(\phi, \psi) = -2\,\mathbf{Im}\left\{\gamma_n^{\phi\psi}\left(Z_{mn}^{\phi\psi}\right)^*\right\}, \tag{17}$$

with $a = 1$, $b = 2$, and $c = 3$ for indexing purposes on the LHS of (16) and (17) (e.g. $M_{mn}(a, b)$ refers to the (1,2) index so that $M_{mn}(1, 2) = 2\,\mathbf{Re}\{\gamma_n^{ab}\left(Z_{mn}^{ab}\right)^*\}$). Finally, we express the γ terms as generalized complex numbers, $\gamma_n^{\phi\psi} = \alpha_n^{\phi\psi} + j\beta_n^{\phi\psi}$, and rewrite (16) and (17) as (18) and (19), respectively:

$$\mathbb{M}_{mn}(\phi, \psi) = 2 \begin{cases} r_{mn}^{\phi\psi} & \text{if } \phi = \psi \\ \alpha_n^{\phi\psi}r_{mn}^{\phi\psi} + \beta_n^{\phi\psi}x_{mn}^{\phi\psi} & \text{if } \phi \neq \psi \end{cases} \tag{18}$$

$$\mathbb{N}_{mn}(\phi,\psi) = 2 \begin{cases} x_{mn}^{\phi\psi} & \text{if } \phi = \psi \\ \alpha_n^{\phi\psi} x_{mn}^{\phi\psi} - \beta_n^{\phi\psi} r_{mn}^{\phi\psi} & \text{if } \phi \neq \psi \end{cases} \quad (19)$$

Eqs. (15) - (19) represent the portion of the *Dist3Flow* equations that govern the relationship between squared voltage magnitudes between adjacent nodes and complex power flow. This system, as it is nonlinear and nonconvex, is difficult to directly incorporate into an OPF formulation without the use of convex relaxations. However, this system can be linearized via making the following assumptions:

A2: $\mathbb{H}_{mn}$ is constant $\forall (m,n) \in \mathcal{E}$
A3: $\gamma_n^{\phi\psi}$ are constant $\forall n \in \mathcal{N}$, $\forall \phi \in \{a,b,c\}$, $\psi \in \{a,b,c\}$, $\phi \neq \psi$

Application of assumptions **A2** and **A3** to the system of (15) - (19) results in a linear model that relates the squared magnitudes of nodal voltages and complex power flows to DER injected power. We refer to the resulting system due to the application of **A2** and **A3** to (15) - (19) as the *LinDist3Flow* magnitude equations.

The *LinDist3Flow* magnitude equations can be further simplified via logical choices for the constant parameters of **A2** and **A3**. Following the analysis presented in [9], we choose $\mathbb{H}_{mn} = [0,\ 0,\ 0]^T\ \forall (m,n) \in \mathcal{E}$. Next we define the parameter σ such that:

$$\sigma = \frac{-1 + j\sqrt{3}}{2}, \quad \sigma^2 = \frac{-1 - j\sqrt{3}}{2}, \quad (20)$$

and assign them to the γ terms according to:

$$\gamma_n^{ab} = \sigma \quad \gamma_n^{bc} = \sigma \quad \gamma_n^{ac} = \sigma^2 \quad \forall n \in \mathcal{N} \quad (21)$$

where clearly $\sigma = 1\angle 120°$ and $\sigma^2 = \sigma^*$. This choice of parameters for **A3** reflects the ratio of nominal voltages at the distribution substation, where, typically, $V_0^a = 1\angle 0°$, $V_0^b = 1\angle 240°$, and $V_0^c = 1\angle 120°$. Choosing the γ terms in this manner highlights the effect of the voltage ratio terms of (18) - (19) in rotating non-diagonal elements of the impedance matrix by $\pm 120°$. With a bit of algebra, it is straightforward to verify that with these choices for **A2** and **A3**, Eqs. (15) - (19) become:

$$\mathbb{Y}_m \approx \mathbb{Y}_n - \mathbb{M}_{mn}\mathbb{P}_n - \mathbb{N}_{mn}\mathbb{Q}_n \quad (22)$$

$$\mathbb{M}_{mn} = \begin{bmatrix} -2r_{mn}^{aa} & r_{mn}^{ab} - \sqrt{3}x_{mn}^{ab} & r_{mn}^{ac} + \sqrt{3}x_{mn}^{ac} \\ r_{mn}^{ba} + \sqrt{3}x_{mn}^{ba} & -2r_{mn}^{bb} & r_{mn}^{bc} - \sqrt{3}x_{mn}^{bc} \\ r_{mn}^{ca} - \sqrt{3}x_{mn}^{ca} & r_{mn}^{cb} + \sqrt{3}x_{mn}^{cb} & -2r_{mn}^{cc} \end{bmatrix} \quad (23)$$

$$\mathbb{N}_{mn} = \begin{bmatrix} -2x_{mn}^{aa} & x_{mn}^{ab} + \sqrt{3}r_{mn}^{ab} & x_{mn}^{ac} - \sqrt{3}r_{mn}^{ac} \\ x_{mn}^{ba} - \sqrt{3}r_{mn}^{ba} & -2x_{mn}^{bb} & x_{bc} + \sqrt{3}r_{mn}^{bc} \\ x_{mn}^{ca} + \sqrt{3}r_{mn}^{ca} & x_{mn}^{cb} - \sqrt{3}r_{mn}^{cb} & -2x_{mn}^{cc} \end{bmatrix} \quad (24)$$

The system of (22) - (24) was incorporated into an OPF formulation used to conduct simulations in this work (discussed in Section III). Notice that in the single phase case, this system reduces to a variant of the *LinDistFlow* equations.

D. Dist3Flow: Angle Equations

We now derive an extension of the *Dist3Flow* system that relates differences in voltage angles between adjacent nodes to complex power flows. This derivation shares many similarities with the analysis of Section II-C. We start by multiplying the voltage at node n by the complex conjugate of (4):

$$\mathbb{V}_n \mathbb{V}_m^* = \mathbb{V}_n \mathbb{V}_n^* + \mathbb{V}_n \mathbb{I}_n^* \mathbb{Z}_{mn}^*. \quad (25)$$

Using the definition of the scalar current $(I_n^\phi)^* = S_n^\phi (V_n^\phi)^{-1} \in \mathbb{C}$, (25) can be rewritten as:

$$\mathbb{V}_n \mathbb{V}_m^* = \mathbb{V}_n \mathbb{V}_n^* + \ldots$$
$$\mathbb{V}_n \begin{bmatrix} S_n^a (V_n^a)^{-1} & S_n^b (V_n^b)^{-1} & S_n^c (V_n^c)^{-1} \end{bmatrix} \mathbb{Z}_{mn}^*. \quad (26)$$

We substitute the previously defined γ terms for $V_n^\phi (V_n^\psi)^{-1}$ to (26), giving:

$$\mathbb{V}_n \mathbb{V}_m^* = \mathbb{V}_n \mathbb{V}_n^* + \begin{bmatrix} S_n^a & \gamma_n^{ab} S_n^b & \gamma_n^{ac} S_n^c \\ \gamma_n^{ba} S_n^a & S_n^b & \gamma_n^{bc} S_n^c \\ \gamma_n^{ca} S_n^a & \gamma_n^{cb} S_n^b & S_n^c \end{bmatrix} \mathbb{Z}_{mn}^*. \quad (27)$$

We now gather the diagonal entries of (27) and place them into a 3×1 vector equation. Here, we write the product of V_n^ϕ and $(V_m^\phi)^*$ in polar form, and apply the definition of $\mathbb{Y}_n$:

$$\begin{bmatrix} |V_n^a||V_m^a| \angle (\theta_n^a - \theta_m^a) \\ |V_n^b||V_m^b| \angle (\theta_n^b - \theta_m^b) \\ |V_n^c||V_m^c| \angle (\theta_n^c - \theta_m^c) \end{bmatrix} = \mathbb{Y}_n + \ldots$$
$$\begin{bmatrix} (Z_{mn}^{aa})^* S_n^a + \gamma_n^{ab}(Z_{mn}^{ab})^* S_n^b + \gamma_n^{ac}(Z_{mn}^{ac})^* S_n^c \\ \gamma_n^{ba}(Z_{mn}^{ba})^* S_n^a + (Z_{mn}^{bb})^* S_n^b + \gamma_n^{bc}(Z_{mn}^{bc})^* S_n^c \\ \gamma_n^{ca}(Z_{mn}^{ca})^* S_n^a + \gamma_n^{cb}(Z_{mn}^{cb})^* S_n^b + (Z_{mn}^{cc})^* S_n^c \end{bmatrix} \quad (28)$$

The left hand side of (28) can be separated into its real and imaginary parts as $\angle (\theta_n^\phi - \theta_m^\phi) = \cos(\theta_n^\phi - \theta_m^\phi) + j \sin(\theta_n^\phi - \theta_m^\phi)$. Taking the imaginary part of (28) and separating the RHS into a matrix of rotated impedance terms multiplying a vector of power at node n results in (29):

$$\begin{bmatrix} |V_n^a||V_m^a| \sin(\theta_n^a - \theta_m^a) \\ |V_n^b||V_m^b| \sin(\theta_n^b - \theta_m^b) \\ |V_n^c||V_m^c| \sin(\theta_n^c - \theta_m^c) \end{bmatrix} = \ldots$$
$$\mathbf{Im} \left\{ \begin{bmatrix} (Z_{mn}^{aa})^* & \gamma_n^{ab}(Z_{mn}^{ab})^* & \gamma_n^{ac}(Z_{mn}^{ac})^* \\ \gamma_n^{ba}(Z_{mn}^{ba})^* & (Z_{mn}^{bb})^* & \gamma_n^{bc}(Z_{mn}^{bc})^* \\ \gamma_n^{ca}(Z_{mn}^{ca})^* & \gamma_n^{cb}(Z_{mn}^{cb})^* & (Z_{mn}^{cc})^* \end{bmatrix} \begin{bmatrix} S_n^a \\ S_n^b \\ S_n^c \end{bmatrix} \right\}. \quad (29)$$

We now follow the same steps taken to taken to transform (14) into (15) - (19), and rewrite (29) in terms of active and reactive power components $\mathbb{P}_n, \mathbb{Q}_n \in \mathbb{C}^3$:

$$\begin{bmatrix} |V_m^a||V_n^a| \sin(\theta_m^a - \theta_n^a) \\ |V_m^b||V_n^b| \sin(\theta_m^b - \theta_n^b) \\ |V_m^c||V_n^c| \sin(\theta_m^c - \theta_n^c) \end{bmatrix} = \frac{1}{2}\mathbb{N}_{mn}\mathbb{P}_n - \frac{1}{2}\mathbb{M}_{mn}\mathbb{Q}_n, \quad (30)$$

with $\mathbb{M}_{mn}$ and $\mathbb{N}_{mn}$ as defined in (18) and (19), respectively. The reader should note that in rewriting (29) as (30) we

multiply both sides by -1, so as to be consistent with the convention in the previous section. The system of (30), (18), and (19) represent the *Dist3Flow* voltage angle equations. Inspection of this extension reveals some interesting properties compared to the *Dist3Flow* voltage magnitude equations of (15), (18), and (19). The RHS of Eqs. (15) and (30) are the real and imaginary parts of the same argument (except for a scaling factor of one-half).

Like the *Dist3Flow* magnitude equations, the system of (30), (18), and (19) are nonlinear and nonconvex and are difficult to incorporate into an OPF. Therefore, we introduce the following three assumptions (it should be noted that **A3** is the same as in II-C, and is applied to both the magnitude and angle equations):

A3: $\gamma_n^{\phi\psi}$ are constant $\forall \phi, \psi \in \{a, b, c\}$, $\phi \neq \psi$, $\forall n \in \mathcal{N}$

A4: $\left|\mathbb{V}_m^\phi\right|$ and $\left|\mathbb{V}_n^\phi\right|$ are constant $\forall \phi \in \{a, b, c\}$, $\forall m, n \in \mathcal{N}$

A5: $\sin\left(\theta_m^\phi - \theta_n^\phi\right) \approx \theta_m^\phi - \theta_n^\phi$, via small angle approximation, $\forall \phi \in \{a, b, c\}$, $\forall (m, n) \in \mathcal{E}$

Application of **A3** to (18) and (19), and **A4** - **A5** to (30) gives (31), the *LinDist3Flow* angle equation (the reader should note that **A4** is **only** applied to the LHS of (30)).

$$\begin{bmatrix} |V_m^a| \, |V_n^a| \, (\theta_m^a - \theta_n^a) \\ |V_m^b| \, |V_n^b| \, (\theta_m^b - \theta_n^b) \\ |V_m^c| \, |V_n^c| \, (\theta_m^c - \theta_n^c) \end{bmatrix} \approx \frac{1}{2}\mathbb{N}_{mn}\mathbb{P}_n - \frac{1}{2}\mathbb{M}_{mn}\mathbb{Q}_n \quad (31)$$

We can also further simplify the *LinDist3Flow* angle equations with proper choice of parameters for **A3** and **A4**. We select the same γ parameters for **A3** as in II-C, and set voltage magnitudes to unity for **A4** such that $\left|V_n^\phi\right| = 1 \ \forall \phi \in \{a, b, c\}$, $n \in \mathcal{N}$, so that (31) becomes (32):

$$\begin{bmatrix} \theta_m^a - \theta_n^a \\ \theta_m^b - \theta_n^b \\ \theta_m^c - \theta_n^c \end{bmatrix} \approx \frac{1}{2}\mathbb{M}_{mn}\mathbb{Q}_n - \frac{1}{2}\mathbb{N}_{mn}\mathbb{P}_n, \quad (32)$$

with $\mathbb{M}_{mn}$ and $\mathbb{N}_{mn}$ defined by (23) and (24), respectively.

E. Discussion and Recap

For clarity, we reiterate the systems of equations we present in this work.

The *Dist3Flow* equations are (8), (15) - (19), and (30).

To obtain the linear *LinDist3Flow* equations, we apply **A1** to (8), **A2** to (15), **A3** to (16) - (19), and **A4** - **A5** to (30), so that (30) becomes (31).

We also consider a special simplified case of the *LinDist3Flow* equations, comprised of (9), (22) - (24), and (32).

III. SIMULATION RESULTS

In this section, we present results of an experiment in which the *LinDist3Flow* equations were incorporated into an OPF with the objective of regulating system voltage magnitudes to within acceptable limits, and minimize the voltage phasor difference between a selected node and a target phasor (we refer to this as voltage phasor tracking). The OPF decision variables were DER real and reactive power injections at select nodes, which were capacity constrained (i.e. four-quadrant resources).

Prior to introducing our OPF problem, we first wish to include a brief note regarding the formulation of the voltage phasor tracking problem as an SDP. In an effort to compare the result of our approach with an optimal effort (i.e. solving an OPF that uses the exact power flow equations), we investigated extending the works of [12]-[13]. Our first approach was to formulate an OPF tracking problem using the L1 norm in the objective function, however we could not obtain a tight relaxation (a rank 1 solution) for even the simplest of cases. Following this, we augmented the OPF presented in [13] by adding equality constraints to prescribe voltage magnitude(s) and phase angle(s) at one or more nodes. Not all choices of reference voltage phasor led to a rank 1 solution however, and we would often need to repeatedly guess to find a suitable reference. Our extension of this work and derivation of constrains can be found in the appendix.

Our experiment was conducted on a modified version of the IEEE 37 node distribution feeder model [21], the topology of which is shown in Fig. 1. Feeder topology, line configuration, line impedance, line length, and spot loads are specified in [21]. Delta to Wye conversions were performed where appropriate. Our simulations omitted the voltage regulator between nodes 799 and 701 in order to study voltage regulation with solely DER dispatch. The voltage regulator and segment was replaced with a segment of configuration 721 (from the IEEE 37 node feeder specification) and length of 1850 feet. Similarly, the transformer between 709 and 755 was replaced with a switch and a 50 foot line segment of configuration 724. This switch separates an intentionally islanded section of the network. Spot loads were increased by a factor of 3 so that voltage magnitudes at nodes far from the substation would be in violation of acceptable bounds in the baseline simulation.

Four-quadrant-capable DER were placed at the following nodes: 702, 704, 725, 724, 729, 732, 735, 737, and 711. We assumed each DER can inject or sink both real and reactive power separately on each phase of the feeder. The DER were constrained by an apparent power capacity limit on each phase of 300 kVA, or 0.12 pu.

In our experiment, voltage magnitudes were constrained to be within $\pm 5\%$ of 1.0 p.u. The voltage at the feeder head was assigned as: $\mathbb{V}_0 = \left[1\angle 0°, \ 1\angle 240°, \ 1\angle 120°\right]^T$ p.u. We incorporated the voltage dependent load model of (3) with parameters $A_{PQ,n}^\phi = 0.9$ and $A_{Z,n}^\phi = 0.1 \ \forall \phi \in \{a, b, c\}$, $\forall n \in \mathcal{N}$.

In this experiment, we considered switching in an islanded node 775 to the network (i.e. closing the switch between the nodes 709 and 775). To minimize sudden and large real or reactive power flows across the switch and disturbances to the network, we desired to match the voltage phasors at node 709 to that of node 775. To this end, we proposed the following OPF to minimize the voltage phasor difference between one or more nodes and the respective reference at each node, while
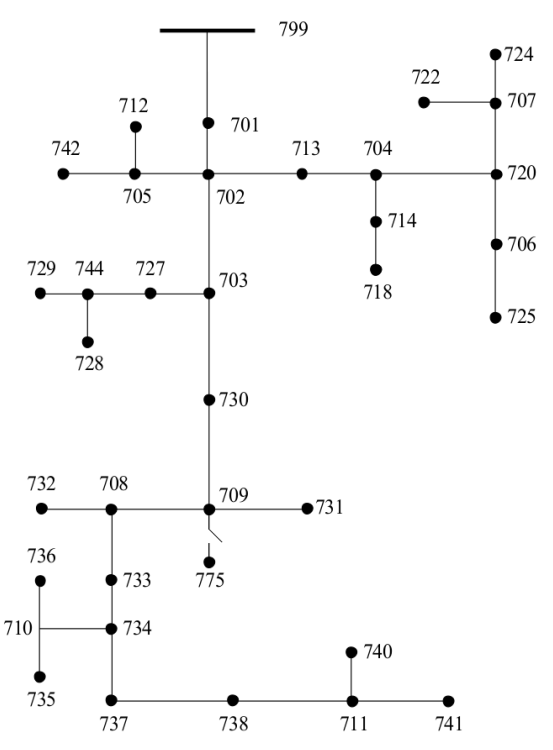
Fig. 1: Modified IEEE 37 node feeder topology. Note the switch between node 709 and node 775.

providing feeder voltage support:

$$\begin{array}{ll} \underset{u_n^\phi, v_n^\phi, y_n^\phi, \theta_n^\phi, P_n^\phi, Q_n^\phi}{\text{minimize}} & \rho_y C_y + \rho_\theta C_\theta + \rho_w C_w \\ \text{subject to} & (3), (9), (22) - (24), (32) \\ & \underline{y} \le y_n^\phi \le \overline{y} \quad \forall \phi \in \{a,b,c\}, \ \forall n \in \mathcal{N}, \\ & \left| w_n^\phi \right| \le \overline{w} \quad \forall \phi \in \{a,b,c\}, \ \forall n \in \mathcal{N}, \end{array}$$
(33)

where
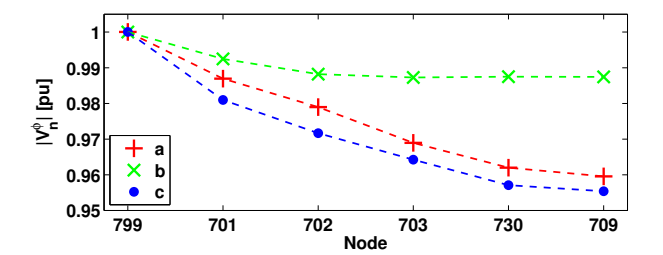
$$C_y = \sum_{n \in \mathcal{N}} \sum_{\phi \in \{a,b,c\}} \left(y_n^\phi - y_{ref,n}^\phi \right)^2,$$
(34)

$$C_\theta = \sum_{n \in \mathcal{N}} \sum_{\phi \in \{a,b,c\}} \left(\theta_n^\phi - \theta_{ref,n}^\phi \right)^2,$$
(35)

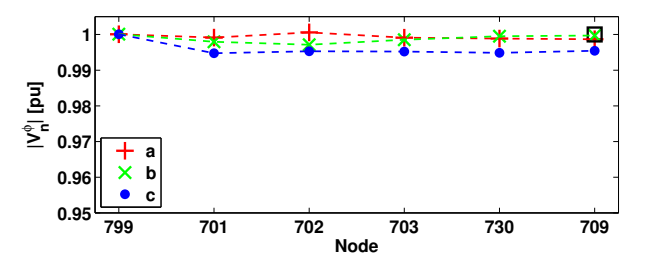$$C_w = \sum_{n \in \mathcal{N}} \sum_{\phi \in \{a,b,c\}} \left| w_n^\phi \right|^2$$
(36)

The OPF objective function is a weighted sum of three terms: C_y is the sum of squared magnitude tracking error for all nodes and phases with an assigned magnitude reference, C_θ is the sum of squared angle tracking error for all nodes and phases with an assigned angle reference, and C_w is the sum of the squared magnitudes of all DER dispatch.

We chose the phasor of node 775 to have unity magnitude ($y_{ref,709}^\phi = 1$, $\phi \in \{a,b,c\}$) and an angle of $0°$, $240°$, and $120°$ for phases a, b and c, respectively ($\theta_{ref,709}^a = 0°$, $\theta_{ref,709}^b = 240°$, and $\theta_{ref,709}^c = 120°$). Finally, the weights in the objective function were chosen as: $\rho_y = 1000$, $\rho_\theta = 100$, $\rho_w = 1$.
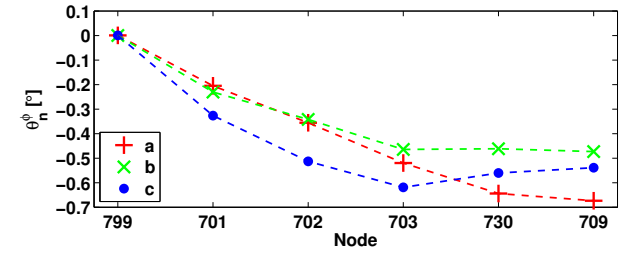

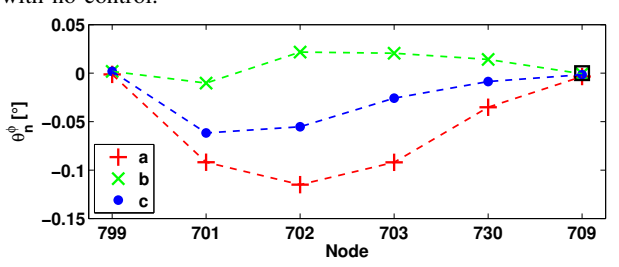**(a)** Voltage magnitude profile on path from node 799 to node 709 with no control.

(b) Voltage magnitude profile on path from node 799 to node 709 with control from (33). The magnitude reference for phases a,b, and c is represented by the black square.

Fig. 2: Comparison of voltage magnitude profiles of base and control cases for phasor reference tracking scenario.

(a) Voltage angle profile on path from node 799 to node 709 with no control.

(b) Voltage angle profile on path from node 799 to node 709 with control from (33). The angle reference for phases a,b, and c is represented by the black square.

Fig. 3: Comparison of voltage angle profiles for phasor reference tracking scenario. Voltage angles for phases $\{a,b,c\}$ are referenced to $0°$ ($120°$ is added to phase b voltage angle and subtracted from phase c voltage angle). The angle reference is referenced to $0°$ in the same manner.

Simulation results, which depict the solution of power flow using the results of (33), are presented in Figs. 2 - 3. The voltage magnitude for phases $\{a,b,c\}$ at nodes along the path from node 799 to node 775 are shown by Fig. 2a (a baseline case with no control applied), and Fig. 2b (power flow results using the solution of (33) - or the "control" case). OPF real and

reactive power dispatches for controlled nodes can be found in Table III. It can clearly be seen that using the dispatch computed by the OPF, the voltage magnitude at node 775 was drastically changed for all three phases and is driven closer to the reference value. Table II shows the resulting voltage magnitudes at node 709 following the application of control. Additionally, note that voltage violations in the baseline case have been corrected. For nodes not depicted in the figures, in the base case simulation all nodes (9 in total) downstream of node 733 had voltage magnitudes lower than 0.95 on phases a and c. These violations were alleviated following the application of control.

The voltage angle on phases $\{a, b, c\}$ for nodes along the path from node 799 to node 709 is given by Fig. 3a for the baseline case, and Fig. 3b for the control case, which shows power flow results using the solution of (33). As can be seen in the figures, the voltage angles were driven extremely close to the respective references. The resultant voltage angles at node 709 for phases $\{a, b, c\}$ can be found in Table II.

TABLE II: COMPARISON OF VOLTAGE PHASOR MAGNITUDES AND PHASE ANGLES AT NODE 709.

Phase		a	b	c
Magnitude Reference	[pu]	1	1	1
Base Magnitude	[pu]	0.9596	0.9874	0.9554
Control Magnitude	[pu]	0.9987	0.9997	0.9954
Angle Reference	[°]	0	240	120
Base Angle	[°]	-0.6731	240.5272	119.4613
Control Angle	[°]	-0.0034	240.9994	119.9984

Inspection of Table II shows, following the application of control, a maximum voltage magnitude error of 0.0046 p.u., and a maximum voltage angle error of 0.0034 °.

TABLE III: OPTIMAL DER DISPATCH FROM (33).

Node	Phase		
	$a\ (w_n^a)$ [pu]	$b\ (w_n^b)$ [pu]	$c\ (w_n^c)$ [pu]
702	-0.0551 - j0.0587	-0.0627 - j0.0197	-0.1079 - j0.0525
704	-0.0551 - j0.0588	-0.0628 - j0.0195	-0.1079 - j0.0525
725	-0.0552 - j0.0588	-0.0628 - j0.0194	-0.1079 - j0.0525
724	-0.0552 - j0.0588	-0.0627 - j0.0194	-0.1079 - j0.0525
729	-0.0797 - j0.0833	-0.0881 - j0.0371	-0.1078 - j0.0528
732	-0.1158 - j0.0314	-0.0539 - j0.0264	-0.1095 - j0.0492
735	-0.1157 - j0.0318	-0.0546 - j0.0260	-0.1095 - j0.0491
737	-0.1157 - j0.0318	-0.0546 - j0.0260	-0.1095 - j0.0491
711	-0.1157 - j0.0320	-0.0549 - j0.0258	-0.1095 - j0.0491

IV. CONCLUSION

Optimization of unbalanced power flow is a challenging topic due to its nonlinear and non-convex nature. While recent works on SDP relaxations [12] - [13] have made OPF formulations for unbalanced systems possible, these approaches suffer from restrictions on the possible objectives and a high-dimensional geometrical complexity that impedes feasibility and uniqueness of the solutions. In an effort to solve problems that cannot be addressed via SDP techniques, in this paper we sought to extend our previous work [15], [16] in developing an approximate model for distribution power flow that could be subsequently incorporated into optimal power flow problems.

To do so, in Section II we developed a model that maps complex power flows into voltage angle differences. It was noted that the complex power/voltage angle relationship shared a similar structure to the complex power/voltage magnitude relationship, in that they incorporated the imaginary part and real part, respectively, of the same vector of complex power flows. Due to this structure, we were able to utilize the linearizing assumptions in our previous efforts to simplify the voltage angle/complex power relationship, thereby extending the *LinDist3Flow* system. The extended *LinDist3Flow* model, henceforth, allowed the formulation of OPF problems that managed the entire voltage phasor, rather than only voltage magnitudes.

Using this linear model, in Section III, we proposed an OPF to manage DER assets to enable "clean" switching in distribution systems (whereby minimal amounts of power flows through the switch after it is closed). To accomplish this, the OPF sought to minimize the voltage phasor difference across a switch that separated a large islanded load and the distribution system. The voltage phasor of the islanded load, which was assumed to be uncontrolled, was treated as a reference signal. The OPF then dispatched DER resources so that the voltage phasor on the feeder-side of the open switch was driven to this reference, while simultaneously maintaining proper voltage profiles in the rest of the system. Simulation results showed the effectiveness of the OPF in driving the selected voltage phasor to meet the target. In so doing, we ensured that, upon closing the switch, minimal amounts of power would flow across the switch resulting in a negligible disturbance in the feeder voltage profile.

The ability to switch components into and out of distribution feeders with minimal impact on system operation presents many opportunities to reconfigure distribution systems for a variety of purposes. Moving forward, we intend to investigate two such applications. First, we plan to study grid reconfiguration in order to better withstand critical grid events (e.g. weather-related or other types of disasters). In anticipation of a critical event, it may be advantageous to alter system topology to maximize the ability to serve critical loads. To solve such a problem, we will most likely need to extend our present OPF formulation into a receding horizon controller, that can optimize over a future time window. Secondly, as "clean" switching may also enable distributed microgrids to coalesce and pool resources to provide ancillary services, we intend to extend this OPF formulation to allow for mixed-integer formulations.

APPENDIX

Extension of Semidefinite OPF of [12], [13]: We start by rewriting the matrix variable $X = vv^*$, where $v = \begin{bmatrix} \mathbb{V}_0^T, & \mathbb{V}_1^T, & \dots & \mathbb{V}_N^T \end{bmatrix}^T$ and $\mathbb{V}_n = \begin{bmatrix} V_n^a, & V_n^b, & V_n^c \end{bmatrix}^T$. Consider a reference magnitude for phase ϕ at node n, Υ_n^ϕ; Adding the following equality constraint to the OPF formulation will

ensure $\left|V_n^\phi\right| = \Upsilon_n^\phi$, as $\left|V_n^\phi\right| = \Upsilon_n^\phi \Rightarrow \left|V_n^\phi\right|^2 = \left(\Upsilon_n^\phi\right)^2 \Rightarrow V_n^\phi\left(V_n^\phi\right)^* = \left(\Upsilon_n^\phi\right)^2$:

$$\text{Tr}\left(\Phi_{V,n}^\phi X\right) = \left(\Upsilon_n^\phi\right)^2 \tag{37}$$

where $\Phi_{V,n}^\phi = e_n^\phi\left(e_n^\phi\right)^T$ as in [12].

Now, consider an off-diagonal entry of X, $X_{n0}^\phi = V_n^\phi\left(V_0^\phi\right)^*$, corresponding to the product of the phasor of phase ϕ at node n, and the complex conjugate of the phasor of phase ϕ at node 0. Here, we express this term in polar form:

$$X_{n0}^\phi = V_n^\phi\left(V_0^\phi\right)^* = \left|V_n^\phi\right|\left|V_0^\phi\right| \angle \left(\theta_n^\phi - \theta_0^\phi\right) \tag{38}$$

Using Euler's rule, we write the the real and imaginary parts of X_{0n}^ϕ in terms of the tangent of $\theta_n^\phi - \theta_0^\phi$:

$$\mathbf{Re}\left\{V_n^\phi\left(V_0^\phi\right)^*\right\}\tan\left(\theta_n^\phi - \theta_0^\phi\right) = \mathbf{Im}\left\{V_n^\phi\left(V_0^\phi\right)^*\right\} \tag{39}$$

The real and imaginary parts of $V_n^\phi\left(V_0^\phi\right)^*$ are defined as:

$$\mathbf{Re}\left\{V_n^\phi\left(V_0^\phi\right)^*\right\} = \frac{1}{2}\left[V_n^\phi\left(V_0^\phi\right)^* + V_0^\phi\left(V_n^\phi\right)^*\right]$$
$$= \frac{1}{2}\left[\text{Tr}\left(\Phi_{V,n0}^\phi X\right) + \text{Tr}\left(\Phi_{V,0n}^\phi X\right)\right] \tag{40}$$

$$\mathbf{Im}\left\{V_n^\phi\left(V_0^\phi\right)^*\right\} = \frac{1}{j2}\left[V_n^\phi\left(V_0^\phi\right)^* - V_0^\phi\left(V_n^\phi\right)^*\right]$$
$$= \frac{1}{j2}\left[\text{Tr}\left(\Phi_{V,n0}^\phi X\right) - \text{Tr}\left(\Phi_{V,0n}^\phi X\right)\right], \tag{41}$$

where $\Phi_{V,n0}^\phi = e_0^\phi\left(e_n^\phi\right)^T$ and $\Phi_{V,0n}^\phi = e_n^\phi\left(e_0^\phi\right)^T$ using the same convention for e_n^ϕ as in [12]. With some matrix algebra, we obtain equality constraints for the phase angle:

$$\text{Tr}\left(\Phi_{\theta,n}^\phi X\right) = 0 \tag{42}$$
$$\Phi_{\theta,n}^\phi = \tan\left(\theta_n^\phi - \theta_0^\phi\right)\left(\Phi_{V,n0}^\phi + \Phi_{V,0n}^\phi\right)$$
$$+ j\left(\Phi_{V,n0}^\phi - \Phi_{V,0n}^\phi\right). \tag{43}$$

In this derivation we reference the phase angle of phase ϕ at node n to that of phase ϕ at node 0. This formulation is easily modified to reference phase angles to a common or arbitrary reference.

The nature of SDPs disallows incorporation of the L2 norm, thus we were unable to formulate (33) as an SDP. However, it is possible to formulate the SDP with an L1 norm minimization. We write an example objective function for an OPF where one node has a voltage magnitude reference:

$$\min_X \sum_{\phi \in \{a,b,c\}} \left|\text{Tr}\left(\Phi_{V,n}^\phi X\right) - \Upsilon_n^\phi\right| \tag{44}$$

This can be extended to a problem with multiple nodes having magnitude references. Similarly, (42) and (43) can be used in the same manner for phase angle references.

REFERENCES

[1] E. M. Stewart, S. V. MacPherson, D. Nakafuji, and T. Aukai, "Analysis of high-penetration levels of photovoltaics into the distribution grid on oahu, hawaii, detailed analysis of heco feeder wf1," NREL subcontract report NREL/SR-5500-54494, Tech. Rep., 2013.

[2] "Voices of experience - insights into advanced distribution management systems," 2015. [Online]. Available: https://www.smartgrid.gov/document/insights_advanced_distribution_management_systems.html

[3] K. Turitsyn, P. Sulc, S. Backhaus, and M. Chertkov, "Options for control of reactive power by distributed photovoltaic generators," *Proceedings of the IEEE*, vol. 99, no. 6, pp. 1063–1073, 2011.

[4] N. Li, G. Qu, and M. Dahleh, "Real-time decentralized voltage control in distribution networks," in *Communication, Control, and Computing (Allerton), 2014 52nd Annual Allerton Conference on*. IEEE, 2014, pp. 582–588.

[5] B. Robbins, C. N. Hadjicostis, A. D. Domínguez-García *et al.*, "A two-stage distributed architecture for voltage control in power distribution systems," *Power Systems, IEEE Transactions on*, vol. 28, no. 2, pp. 1470–1482, 2013.

[6] B. Zhang, A. D. Dominguez-Garcia, and D. Tse, "A local control approach to voltage regulation in distribution networks," in *North American Power Symposium (NAPS), 2013*. IEEE, 2013, pp. 1–6.

[7] M. Farivar, C. R. Clarke, S. H. Low, and K. M. Chandy, "Inverter var control for distribution systems with renewables," in *IEEE International Conference on Smart Grid Communications (SmartGridComm)*. IEEE, 2011, pp. 457–462.

[8] A. Lam, B. Zhang, A. Dominguez-Garcia, and D. Tse, "Optimal distributed voltage regulation in power distribution networks," *arXiv preprint arXiv:1204.5226*, 2012.

[9] M. E. Baran and F. F. Wu, "Optimal sizing of capacitors placed on a radial distribution system," *IEEE Transactions on Power Delivery*, vol. 4, no. 1, pp. 735–743, 1989.

[10] D. B. Arnold, M. Negrete-Pincetic, M. D. Sankur, D. M. Auslander, and D. S. Callaway, "Model-free optimal control of var resources in distribution systems: An extremum seeking approach," *IEEE Transactions on Power Systems*, vol. PP, pp. 1–11, 2015.

[11] W. H. Kersting, *Distribution system modeling and analysis*. CRC press, 2012.

[12] E. Dall'Anese, G. B. Giannakis, and B. F. Wollenberg, "Optimization of unbalanced power distribution networks via semidefinite relaxation," in *North American Power Symposium (NAPS), 2012*. IEEE, 2012, pp. 1–6.

[13] E. Dall'Anese, H. Zhu, and G. Giannakis, "Distributed optimal power flow for smart microgrids," *Smart Grid, IEEE Transactions on*, vol. 4, no. 3, pp. 1464–1475, 2013.

[14] R. Louca, P. Seiler, and E. Bitar, "Nondegeneracy and inexactness of semidefinite relaxations of optimal power flow," *arXiv*, vol. 1441.4663v1, 2014.

[15] D. B. Arnold, M. D. Sankur, R. Dobbe, K. Brady, D. S. Callaway, and A. Von Meier, "Optimal dispatch of reactive power for voltage regulation and balancing in unbalanced distribution systems," *IEEE Power and Energy Society General Meeting, accepted*, 2016.

[16] M. D. Sankur, R. Dobbe, E. Stewart, D. S. Callaway, and D. B. Arnold, "A linearized power flow model for optimization in unbalanced distribution systems," *arXiv*, vol. 1606.04492, 2016.

[17] "Grid modernization multi-year program plan," http://energy.gov/sites/prod/files/2016/01/f28/Grid%20Modernization%20Multi-Year%20Program%20Plan.pdf.

[18] "Quadrennial energy review: First installment," urlhttp://energy.gov/epsa/downloads/quadrennial-energy-review-first-installment, online; April-2015.

[19] L. F. Ochoa and D. H. Wilson, "Angle constraint active management of distribution networks with wind power," in *Innovative Smart Grid Technologies Conference Europe (ISGT Europe), 2010 IEEE PES*. IEEE, 2010, pp. 1–5.

[20] D. Wang, D. Wilson, S. Venkata, and G. C. Murphy, "Pmu-based angle constraint active management on 33kv distribution network," in *Electricity Distribution (CIRED 2013), 22nd International Conference and Exhibition on*. IET, 2013, pp. 1–4.

[21] "Ieee distribution test feeders," http://ewh.ieee.org/soc/pes/dsacom/testfeeders/index.html, online; accessed May-2015.